

Phononic thermal transport along graphene grain boundaries

Zhen Tong,¹ Alessandro Pecchia,² ChiYung Yam,^{1,3} Traian Dumitrică,^{4,*} and Thomas Frauenheim^{3,1,5,†}

¹Shenzhen JL Computational Science and Applied Research Institute, Shenzhen 518131, China.

²CNR-ISMN, Via Salaria km 29.300, Monterotondo 00017, Rome, Italy

³Beijing Computational Science Research Center, Beijing 100193, China

⁴Department of Mechanical Engineering, University of Minnesota, Minnesota 55455, United States of America

⁵Bremen Center for Computational Materials Science, University of Bremen, Bremen 2835, Germany

We reveal that phononic thermal transport in graphene is not immune to grain boundaries (GBs) aligned along the direction of the temperature gradient. Non-equilibrium molecular dynamics simulations uncover a large reductions in the phononic thermal conductivity (κ_p) along linear ultra-narrow GBs comprising periodically-repeating pentagon-heptagon dislocations. Green's function calculations and spectral energy density analysis indicate that κ_p is the complex manifestation of the periodic strain field, which behaves as a reflective diffraction grating with both diffuse and specular phonon reflections, and represents a source of anharmonic phonon-phonon scattering. Our findings provide new insights into the integrity of the phononic thermal transport in GB graphene.

Next generation of high-performance electronics and sensors require materials with high thermal conductivity able to spread effectively the high density of Joule heat generation along and across various thin films and substrates [1, 2]. Two-dimensional materials like graphene [3] are very attractive for these applications as they are relatively immune to detrimental size effects on basal-plane thermal conductivity. This is because the highly anisotropic phonon group velocity reduces the impact of scattering by the top and bottom surfaces [4, 5]. Nevertheless, thermal transport is significantly impacted [6] by the defects occurring during synthesis. In this respect, the widely-used chemical vapor deposition (CVD) [7] unavoidably produces grain boundaries (GBs). As domains nucleate randomly on substrates, their CVD growth and coalescence result in formation of GBs [8–11].

GBs are imagined as periodic arrays of dislocations [12]. In graphene, GBs are strings of pentagon-heptagon (5-7) edge dislocations [9, 13–15] and their organization can give rise to diverse GB shapes. While in general the thermal gradient can have an arbitrary orientation with respect to the GB line [16, 17], only transport *across* GBs is perceived to significantly impact κ_p . Green's function (GF) calculations [18, 19] obtained that heat transmission across the GB can be significantly influenced by the GB structure, size, and shape. Non-equilibrium molecular dynamics (NEMD) simulations [20–22] revealed a discontinuity in the temperature (T) profile across GBs and that higher dislocation densities lead to lower κ_p .

In this Letter, we reveal that thermal transport is not immune to GBs oriented *along* the thermal gradient. By way of NEMD simulations with LAMMPS [23], we report κ_p reduction along GBs with various 5-7 dislocation densities and length scales L covering ballistic and dif-

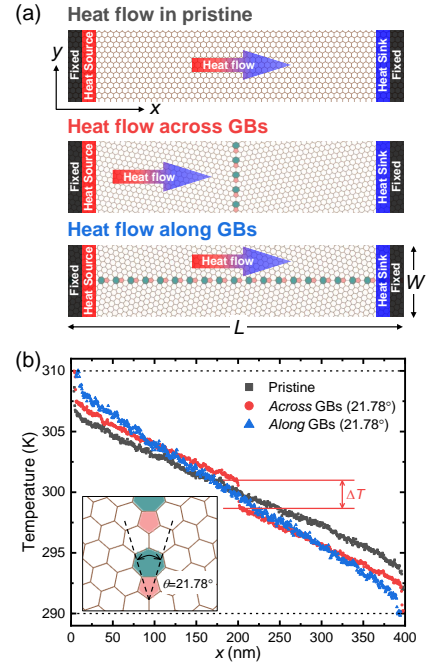


FIG. 1: (a) NEMD setup for pristine and GB graphene with $\theta=21.78^\circ$. (b) Computed T profiles.

usive transport, in systems of up to 59,0512 carbon (C) atoms treated with the optimized Tersoff potential [24]. To gain a clear understanding, we also conducted GF calculations of phononic transmission and conductance, and spectral energy density (SED) calculations to quantify phonon relaxation times. The uncovered κ_p behavior with a non-monotonic dependence on 5-7 defect density is unaccounted for by the classical Klemens theory [6].

The NEMD setup is presented in Fig. 1(a). Two-unit

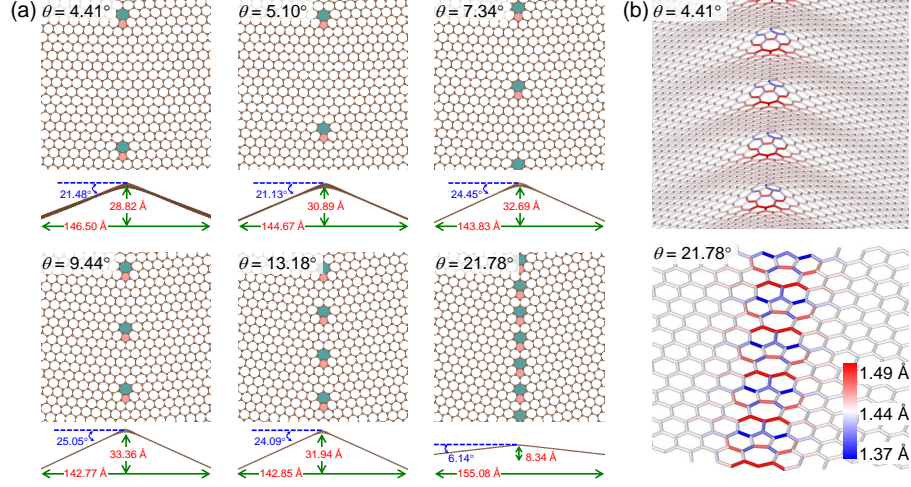


FIG. 2: (a) The top and side views of 6 considered GBs with different θ . (b) Bird's eye view along two GB lines.

cells at each end were kept fixed throughout simulation and ten other neighboring unit cells were designated as “hot” and “cold” baths maintained at the temperatures $T_h=310 \text{ K}$ and $T_c=290 \text{ K}$, respectively. At steady-state, the heat flux \dot{Q} was calculated as the difference of the rate of the kinetic energy extraction from the two reservoirs $\dot{Q} = 0.5(\dot{Q}_h - \dot{Q}_c)$, where \dot{Q}_h and \dot{Q}_c are the instantaneous heat currents flowing into and away from the “hot” and “cold” baths. The angular brackets indicate a statistical average taken after the steady state was reached. Graphene edges [25] can significantly impact thermal transport [16]. The application of periodic boundary conditions along y eliminates the lateral edges and allows for the simulation of the thermal transport perpendicular to a single GB line and along antiparallel GB lines (i.e, the 5-7 defect lines run parallel to each other but with opposite directionality) separated by the lateral periodicity W . Therefore, differences in calculated T profiles, Fig. 1(b), can be attributed solely to GBs.

The NEMD calculations of Fig. 1(b) at $L = 400 \text{ nm}$ and $W = 15.5 \text{ nm}$ reveal a stark difference in the T profiles across and along the considered GBs, which comprises aligned 5-7 defects separated by one hexagonal ring. In agreement with Azizi *et al.* [22], there is a sharp temperature drop $\Delta T = 2.2 \text{ K}$, corresponding to a thermal resistance $\Delta T/\dot{q}$ of $0.035 \text{ Km}^2/\text{GW}$ across this GB. Here \dot{q} is \dot{Q} per cross-sectional area (defined here based on the 0.33 nm thickness of graphene [26, 27]). Nevertheless, along the GB line, the T profile is smooth and resembles the one obtained for the pristine graphene. By thermal symmetry, the GB lines oriented along the heat flow are adiabatic lines. If heat transfer was purely one-dimensional, then κ_p would hardly be impacted along GBs. Nevertheless, the extracted $\kappa_p = -\dot{q}(dT/dx)$, reveal a nearly 50% reduction (633.2 W/mK vs. $1,259.4 \text{ W/mK}$) demonstrating that through

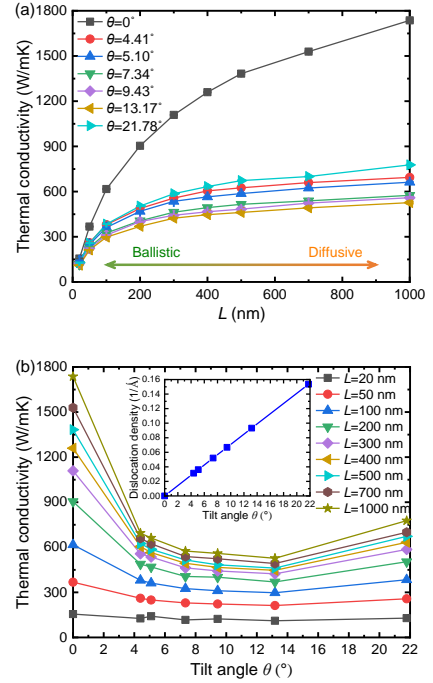


FIG. 3: NEMD computed (a) κ_p vs. L at 300 K in graphene and along GBs with different θ . (b) κ_p vs. θ for different L . The inset shows the 5-7 density vs. θ .

the two-dimensionality of the heat transport κ_p is significantly impacted even by such linear ultra-narrow GBs.

We have checked the robustness of our result by extensive NEMD, see Fig. S2(b), which considered symmetric tilt GB systems with similar widths W but different L and spread out linear arrangements of the 5-7 defects, which decrease the tilt angles θ [28] formed by the crystallographic directions of the neighboring domains, Fig. 2(a). Additionally, a 5-7 pair introduces local off-plane

elevations [29] as a way of relieving the strain stored in the dislocation core. The resulting “bumpy” landscape with a rather blazed profile is visible in Fig. 2(b) for the $\theta=4.41^\circ$ GB. On the same figure, it can be also seen that the C-C bond extension and compression deformations are strongly localized around the 5-7 cores. The off-plane displacement are opposite in neighboring GB lines, such stable ripple structures are formed. As shown in the side views of Fig. 2(a), the ripples acquire significant amplitudes of $15 \pm 1.5 \text{ \AA}$. Only for $\theta=21.78^\circ$, the closeness of the 5-7 cores inhibits their off-plane displacements reducing the ripple amplitude to only 4.17 \AA . For this case, the C-C bond deformations are continuous along the GB line, Fig. 2(b). Overall, in all of the rippled structures of Fig. 2 found by energy minimizations, the C-C bonds away from the GB lines are undeformed; the axial prestrain is also very small; it varies monotonically with θ , from -0.2% ($\theta=4.41^\circ$) to 0.1% ($\theta=21.78^\circ$), see Fig. S1(b).

Figure 3(a) demonstrates that the differences between κ_p in pristine ($\theta = 0$) [30, 31] and along GBs with different θ remain significant at different L . In the pristine case, the initial linear increase of κ_p ($L < 100 \text{ nm}$) is a signature of pure ballistic behavior, while the subsequent lowering of the rate of increase in κ_p at $L \sim 100 \text{ nm}$ signals that the thermal transport enters into a diffusive regime. κ_p is expected to increase in a logarithmically divergent manner at L much larger than the average phonon mean free path ($\sim 775 \text{ nm}$ at $T = 300 \text{ K}$) [30, 31]. Along GBs, κ_p initially increases with a smaller slope than in the pristine case. At larger L , κ_p becomes convergent at $L \sim 400 \text{ nm}$ when the diffusive regime settles in. At the largest considered $L = 1 \mu\text{m}$, the κ_p reduction is of $\sim 60\%$ or larger with respect to the pristine case. While the dislocation density increases with θ , κ_p displays non-monotonic variations, which are more pronounced for $L > 100 \text{ nm}$, Fig. 3(b): κ_p decreases from $\theta = 4.41^\circ$ up to $\theta = 13.18^\circ$ but presents an anomalous enhancement at $\theta = 21.78^\circ$, where the 5-7 density is largest.

To gain insight into the mechanism of κ_p reduction, we have pursued complementary GF investigations. As in NEMD, we have partitioned the system into “hot” bath, device region, and “cold” bath, Fig. 1(a), such as the GB lines extend in all regions. The dynamical matrix D was computed using the same optimized Tersoff potential [24] with a finite difference scheme of the atomic forces, not accounting for finite temperature phonon softening effects owing to anharmonicity. We computed the ballistic transport for $\theta=4.41^\circ$, 13.18° and 21.78° and compared them to the pristine graphene. The conductance g is evaluated within the Landauer approach in terms of the transmission coefficient, $t_p(\omega)$, [32]

$$g = \frac{\hbar^2}{2\pi k_B T^2} \int \omega^2 \frac{e^{\frac{\hbar\omega}{k_B T}}}{(e^{\frac{\hbar\omega}{k_B T}} - 1)^2} t_p(\omega) d\omega, \quad (1)$$

where k_B and $\hbar = h/2\pi$ are the Boltzmann and the

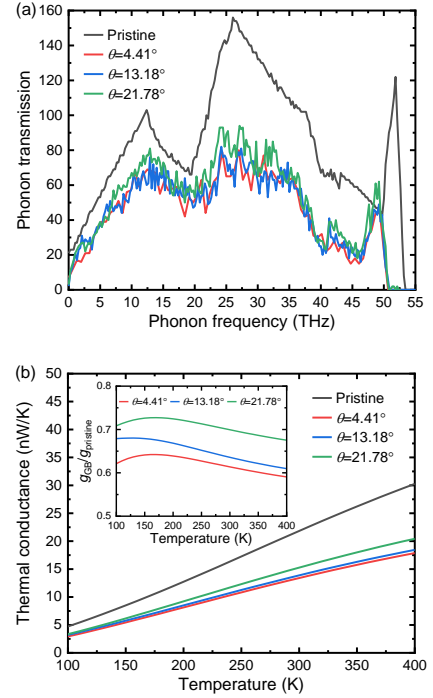


FIG. 4: GF computed (a) phonon transmissions and (b) thermal conductances in pristine and along GB graphene. Inset shows GB conductances with respect to graphene.

Planck constants, respectively. $t_p(\omega)$, in turn, is computed [33] based on D , as $t_p = \text{Tr}[G^r \Gamma_L G^a \Gamma_R]$. The retarded GF is given by $G^r(\omega) = [\omega^2 - D - \Sigma_L^r - \Sigma_R^r]^{-1}$ and $\Gamma_{L,R}$ are the broadening functions, $\Gamma_{L/R} = i[\Sigma_{L/R}^r - \Sigma_{L/R}^a]$, for the “hot” and “cold” contacts.

At $L = 10 \text{ nm}$ considered here, transport is coherent and influenced by the elastic scattering onto the GBs. Plots of $t_p(\omega)$ at different θ are shown in Fig. 4(a). Consistent with NEMD, t_p in pristine graphene is higher than in GBs and yields a higher g value, Fig. 4(b). The conductance is ballistic as reflected in the integer values of t_p , depending on the number of phonon states at each ω . Surprisingly, the $t_p(\omega)$ reduction by GBs is inversely proportional to the 5-7 density (i.e., t_p is largest for $\theta=21.78^\circ$ and smallest for $\theta=4.41^\circ$). This dependence uncovers the strain field periodicity effect, which operates as a diffraction grating onto the traveling phonons. Through elastic scattering on the strain around the 5-7 cores, reflective diffraction spectra of various orders take place. On one hand, for $\theta=21.78^\circ$, strain is continuous along the GB line, Fig. 2(b). Diffraction is dominated by the zero-order, which is associated with a specular reflection and larger group velocity. On the other hand, for $\theta=4.41^\circ$ GB which has lowest g , the 5-7 defects are $\sim 3.2 \text{ nm}$ apart. Destructive interferences introduce stronger phonon localization, which is associated to diffuse reflections and manifests into important thermal resistivity contributions. These important higher diffraction orders

are not considered by Klemens [6, 34]. This situation reminds of the κ_p reduction along central screw dislocations located in nanowires [35, 36], an effect also not captured by the classical theory [6]. By introducing periodic nm-scale grooves onto the nanowire surface [37], κ_p could be further reduced through localization of the phonons that were specularly reflected by the dislocation core.

In summary, the GF calculations obtained that the resistive contributions caused by the diffuse GB reflection scale inversely with the defect density. The g reductions are seen also in the inset of Fig. 4(b), which shows $g_{\text{GB}}/g_{\text{pristine}}$ as a function of T , with g_{GB} and g_{pristine} being g for a given GB and graphene pristine, respectively.

As transport advances into the diffusive regime, the decay of heat carrying phonons by inelastic scatterings becomes increasingly important. Recalling that in a phonon gas model, thermal conductivity is $\kappa_p = \sum_{\lambda} c_{\lambda} v_{\lambda}^2 \tau_{\lambda}$, where c_{λ} , v_{λ} , and τ_{λ} are the specific heat capacity, phonon group velocity, and phonon relaxation time of phonon mode λ , respectively. Figure 5(a) shows τ_{λ} , as calculated by SED scheme [35, 38] and room-temperature equilibrium MD runs. When compared to pristine graphene, GBs lead to significant τ_{λ} reductions. For the “bumpy” GBs, τ_{λ} decreases with the increase in defect density. This dependence is opposite to the one for the ballistic phonon transmission delineated above, and explains the crossover in κ_p as transport advances into the diffusive regime. However, for $\theta = 21.78^\circ$ GB, where t_p is largest compared to other GBs, we also find the largest τ_{λ} in Fig. 5(a). This concerted behavior explains the consistently larger κ_p values for $\theta = 21.78^\circ$ GB with respect to the other considered GBs, Fig. 3(b). The key role of τ_{λ} is further supported in Fig. 5(b) by the lattice dynamics [39] computed v_{λ} , which is another key contributor to κ_p . While for some phonon modes v_{λ} decreases in $\theta = 21.78^\circ$ GB, it remains unchanged for the acoustic phonon modes, which are playing a main role in thermal conduction. Therefore, the weaker phonon scattering in $\theta = 21.78^\circ$ GB (as reflected by the larger τ_{λ}) and not an enhancement of v_{λ} is the mechanism behind the anomalous κ_p behavior. We associate the weaker anharmonic scattering presented in $\theta = 21.78^\circ$ GB to the flatter landscape along the GB line. The 5-7 off-plane distortions at the other θ are enhancing anharmonic scattering as they locally couple the in-plane and out-of-plane degrees of freedom [19], which are otherwise decoupled [40].

In conclusion, we uncovered that through the two-dimensionality of the heat transfer, κ_p along linear ultranarrow GBs is significantly affected. The explanation for the κ_p reduction with the defect density goes beyond the simple phonon specular reflection accounted for by Klemens [6, 34]. κ_p alongs GB with 21.78° is largest, which is opposed to the expected deterioration of thermal transport at larger dislocation density [19]. The κ_p boost is caused by a diffraction grating effect of the GB strain field periodicity, which leads to a specular scatter-

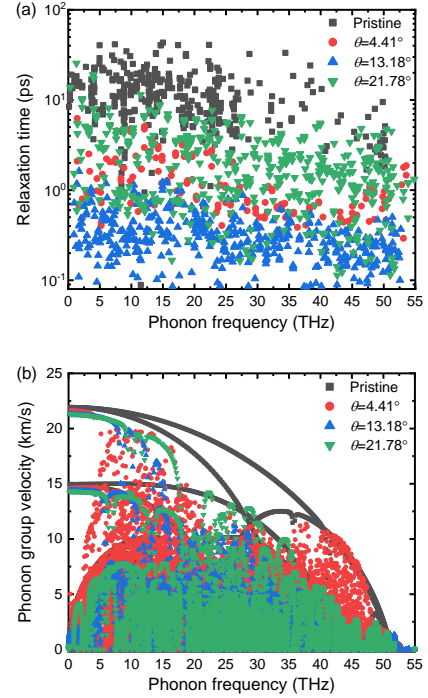


FIG. 5: MD calculated (a) phonon relaxation times and (b) phonon group velocity in pristine and GB graphene.

ing, and to a reduced anharmonic scattering associated to the flatter GB landscape. As the 5-7 defects become sparse and “bumpy”, elastic scattering on GB becomes diffusive, while anharmonic scattering is enhanced. Even for the less dense case of $\theta = 4.14^\circ$ GB, where the 5-7 defects are about 3.2 nm apart, the κ_p reduction remains substantial ($\sim 60\%$ for $L=1 \mu\text{m}$). Our findings provide insights into the thermal response of GB graphene that are intrinsic to the CVD method [7], which currently is the main approach to manufacture graphene for high-performance electronics and sensors applications.

SUPPLEMENTARY MATERIAL

Details on information of GBs, NEMD simulations, SED calculations, phonon transmission.

ACKNOWLEDGMENTS

Simulations were preformed at the Tainhe2-JK of Beijing Computational Science Research Center (CSRC). Z.T. acknowledges the support by China Postdoctoral Science Foundation (Grant No. 2020M680127), Guangdong Basic and Applied Basic Research Foundation (Grants No. 2020A1515110838 and No. 2021A1515011688), and Shenzhen Science and Technology Program (Grant No. RCBS20200714114919142). T.D. and T.F. acknowledge support from DFG FR-2833/7. T.F. acknowledges support from the National Natural Science Foundation of China (Grant No. U1930402).

REFERENCES

-
- * Electronic address: dtraian@umn.edu
- † Electronic address: thomas.frauenheim@bccms.uni-bremen.de
- [1] E. Pop, *Energy dissipation and transport in nanoscale devices*, *Nano Research* **3**, 147 (2010).
 - [2] A. L. Moore and L. Shi, *Emerging challenges and materials for thermal management of electronics*, *Materials Today* **17**, 163 (2014).
 - [3] K. S. Novoselov, *Electric Field Effect in Atomically Thin Carbon Films*, *Science* **306**, 666 (2004).
 - [4] I. Jo, M. T. Pettes, E. Ou, W. Wu, and L. Shi, *Basal-plane thermal conductivity of few-layer molybdenum disulfide*, *Applied Physics Letters* **104**, 201902 (2014).
 - [5] Y. Ni, J. Jiang, E. Meletis, and T. Dumitrică, *Thermal transport across few-layer boron nitride encased by silica*, *Applied Physics Letters* **107**, 031603 (2015).
 - [6] P. G. Klemens, *The scattering of low-frequency lattice waves by static imperfections*, *Proceedings of the Physical Society. Section A* **68**, 1113 (1955).
 - [7] T. Dumitrică, S. Kodambaka, and S. Jun, *Synthesis, electromechanical characterization, and applications of graphene nanostructures*, *Journal of Nanophotonics* **6**, 1 (2012).
 - [8] Q. Yu, L. A. Jauregui, W. Wu, R. Colby, J. Tian, Z. Su, H. Cao, Z. Liu, D. Pandey, D. Wei, *et al.*, *Control and characterization of individual grains and grain boundaries in graphene grown by chemical vapour deposition*, *Nature Materials* **10**, 443 (2011).
 - [9] P. Y. Huang, C. S. Ruiz-Vargas, A. M. van der Zande, W. S. Whitney, M. P. Levendorf, J. W. Kevek, S. Garg, J. S. Alden, C. J. Hustedt, Y. Zhu, J. Park, P. L. McEuen, and D. A. Muller, *Grains and grain boundaries in single-layer graphene atomic patchwork quilts*, *Nature* **469**, 389 (2011).
 - [10] J. An, E. Voelkl, J. W. Suk, X. Li, C. W. Magnuson, L. Fu, P. Tiemeijer, M. Bischoff, B. Freitag, E. Popova, and R. S. Ruoff, *Domain (Grain) Boundaries and Evidence of "Twinlike" Structures in Chemically Vapor Deposited Grown Graphene*, *ACS Nano* **5**, 2433 (2011).
 - [11] O. V. Yazyev and Y. P. Chen, *Polycrystalline graphene and other two-dimensional materials*, *Nature Nanotechnology* **9**, 755 (2014).
 - [12] W. T. Read and W. Shockley, *Dislocation models of crystal grain boundaries*, *Physical Review* **78**, 275 (1950).
 - [13] H. F. Bettinger, T. Dumitrică, G. E. Scuseria, and B. I. Yakobson, *Mechanically induced defects and strength of bn nanotubes*, *Physical Review B* **65**, 041406 (2002).
 - [14] K. Kim, Z. Lee, W. Regan, C. Kisielowski, M. F. Crommie, and A. Zettl, *Grain boundary mapping in polycrystalline graphene*, *ACS Nano* **5**, 2142 (2011).
 - [15] P. Nemes-Incze, P. Vancsó, Z. Osváth, G. I. Márk, X. Jin, Y.-S. Kim, C. Hwang, P. Lambin, C. Chapelier, and L. PéterBiró, *Electronic states of disordered grain boundaries in graphene prepared by chemical vapor deposition*, *Carbon* **64**, 178 (2013).
 - [16] T.-H. Liu, S.-C. Lee, C.-W. Pao, and C.-C. Chang, *Anomalous thermal transport along the grain boundaries of bicrystalline graphene nanoribbons from atomistic simulations*, *Carbon* **73**, 432 (2014).
 - [17] A. Fox, U. Ray, and T. Li, *Thermal conductivity of graphene grain boundaries along arbitrary in-plane directions: A comprehensive molecular dynamics study*, *Journal of Applied Physics* **125**, 015101 (2019).
 - [18] A. Y. Serov, Z.-Y. Ong, and E. Pop, *Effect of grain boundaries on thermal transport in graphene*, *Applied Physics Letters* **102**, 033104 (2013).
 - [19] L. M. Sandonas, H. Sevinçli, R. Gutierrez, and G. Cuniberti, *First-Principle-Based Phonon Transport Properties of Nanoscale Graphene Grain Boundaries*, *Advanced Science* **5**, 1700365 (2018).
 - [20] A. Bagri, S.-P. Kim, R. S. Ruoff, and V. B. Shenoy, *Thermal transport across Twin Grain Boundaries in Polycrystalline Graphene from Nonequilibrium Molecular Dynamics Simulations*, *Nano Letters* **11**, 3917 (2011).
 - [21] A. Cao and J. Qu, *Kapitza conductance of symmetric tilt grain boundaries in graphene*, *Journal of Applied Physics* **111**, 053529 (2012).
 - [22] K. Azizi, P. Hirvonen, Z. Fan, A. Harju, K. R. Elder, T. Ala-Nissila, and S. M. V. Allaei, *Kapitza thermal resistance across individual grain boundaries in graphene*, *Carbon* **125**, 384 (2017).
 - [23] S. Plimpton, *Fast Parallel Algorithms for Short-Range Molecular Dynamics*, *Journal of Computational Physics* **117**, 1 (1995).
 - [24] L. Lindsay and D. A. Broido, *Optimized Tersoff and Brenner empirical potential parameters for lattice dynamics and phonon thermal transport in carbon nanotubes and graphene*, *Physical Review B* **81**, 205441 (2010).
 - [25] V. Barone, O. Hod, and G. E. Scuseria, *Electronic structure and stability of semiconducting graphene nanoribbons*, *Nano Letters* **6**, 2748 (2006).
 - [26] B. Mortazavi and S. Ahzi, *Thermal conductivity and tensile response of defective graphene: A molecular dynamics study*, *Carbon* **63**, 460 (2013).
 - [27] H. Wei, H. Bao, and X. Ruan, *Genetic algorithm-driven discovery of unexpected thermal conductivity enhancement by disorder*, *Nano Energy* **71**, 104619 (2020).
 - [28] O. V. Yazyev and S. G. Louie, *Topological defects in graphene: Dislocations and grain boundaries*, *Physical*

- Review B **81**, 195420 (2010).
- [29] F. Banhart, J. Kotakoski, and A. V. Krashenninnikov, *Structural Defects in Graphene*, [ACS Nano](#) **5**, 26 (2011).
 - [30] S. Ghosh, I. Calizo, D. Teweldebrhan, E. P. Pokatilov, D. L. Nika, A. A. Balandin, W. Bao, F. Miao, and C. N. Lau, *Extremely high thermal conductivity of graphene: Prospects for thermal management applications in nano-electronic circuits*, [Applied Physics Letters](#) **92**, 151911 (2008).
 - [31] X. Xu, L. F. C. Pereira, Y. Wang, J. Wu, K. Zhang, X. Zhao, S. Bae, C. Tinh Bui, R. Xie, J. T. L. Thong, B. H. Hong, K. P. Loh, D. Donadio, B. Li, and B. Özyilmaz, *Length-dependent thermal conductivity in suspended single-layer graphene*, [Nature Communications](#) **5**, 3689 (2014).
 - [32] L. Medrano Sandomas, D. Teich, R. Gutierrez, T. Lorenz, A. Pecchia, G. Seifert, and G. Cuniberti, *Anisotropic Thermoelectric Response in Two-Dimensional Puckered Structures*, [Journal of Physical Chemistry C](#) **120**, 18841 (2016).
 - [33] L. M. Sandomas, R. Gutierrez, A. Pecchia, A. Croy, and G. Cuniberti, *Quantum phonon transport in nanomaterials: Combining atomistic with non-equilibrium green's function techniques*, [Entropy](#) **21**, 735 (2019).
 - [34] M. Omini and A. Sparavigna, *Role of grain boundaries as phonon diffraction gratings in the theory of thermal conductivity*, [Physical Review B](#) **61**, 6677 (2000).
 - [35] Y. Ni, S. Xiong, S. Volz, and T. Dumitrică, *Thermal Transport Along the Dislocation Line in Silicon Carbide*, [Physical Review Letters](#) **113**, 124301 (2014).
 - [36] S. Xiong, J. Ma, S. Volz, and T. Dumitrică, *Thermally-active screw dislocations in si nanowires and nanotubes*, [Small](#) **10**, 1756 (2014).
 - [37] J. Al-Ghalith, Y. Ni, and T. Dumitrică, *Nanowires with dislocations for ultralow lattice thermal conductivity*, [Physical Chemistry Chemical Physics](#) **18**, 9888 (2016).
 - [38] J. A. Thomas, J. E. Turney, R. M. Iutzi, C. H. Amon, and A. J. H. McGaughey, *Predicting phonon dispersion relations and lifetimes from the spectral energy density*, [Physical Review B](#) **81**, 081411(R) (2010).
 - [39] J. D. Gale and A. L. Rohl, *The General Utility Lattice Program (GULP)*, [Molecular Simulation](#) **29**, 291 (2003).
 - [40] D.-B. Zhang, E. Akatyeve, and T. Dumitrică, *Bending ultrathin graphene at the margins of continuum mechanics*, [Physical Review Letters](#) **106**, 255503 (2011).